ACS APPLIED MATERIALS & INTERFACES

Letter

www.acsami.org

Band Engineered Epitaxial 3D GaN-InGaN Core–Shell Rod Arrays as an Advanced Photoanode for Visible-Light-Driven Water Splitting

Lorenzo Caccamo,[†] Jana Hartmann,[†] Cristian Fàbrega,[‡] Sonia Estradé,[§,∥] Gerhard Lilienkamp,[⊥] Joan Daniel Prades,[§] Martin W. G. Hoffmann,[†] Johannes Ledig,[†] Alexander Wagner,[†] Xue Wang,[†] Lluis Lopez-Conesa,[§,▽] Francesca Peiró,[§] José Manuel Rebled,[§] Hergo-Heinrich Wehmann,[†] Winfried Daum,[⊥] Hao Shen,*[,†] and Andreas Waag*[,†]

[†]Institute for Semiconductor Technology, TU Braunschweig, Hans-Sommer-Strasse 66, Braunschweig 38106, Germany

[‡]Catalonia Institute for Energy Research, Jardins de les Dones de Negre 1, Barcelona 08930, Spain

[§]Department d'Electrònica, Universitat de Barcelona, c/Martí Franquès 1, Barcelona 08028, Spain

[⊥]Institute of Energy Research and Physical Technologies, TU Clausthal, Leibnizstrasse 4, Clausthal-Zellerfeld 38678, Germany

[∥]TEM-MAT, CCiTUB, Solé i Sabarís 1, Barcelona 08028, Spain

[▽]Institut de Ciència de Materials de Barcelona (ICMAB - CSIC), Campus UAB, Bellaterra 08193, Spain

Supporting Information

ABSTRACT: 3D single-crystalline, well-aligned GaN-InGaN rod arrays are fabricated by selective area growth (SAG) metal–organic vapor phase epitaxy (MOVPE) for visible-light water splitting. Epitaxial InGaN layer grows successfully on 3D GaN rods to minimize defects within the GaN-InGaN heterojunctions. The indium concentration (In ∼ 0.30 ± 0.04) is rather homogeneous in InGaN shells along the radial and longitudinal directions. The growing strategy allows us to tune the band gap of the InGaN layer in order to match the visible absorption with the solar spectrum as well as to align the semiconductor bands close to the water redox potentials to achieve high efficiency. The relation between structure, surface, and photoelectrochemical property of GaN-InGaN is explored by transmission electron microscopy (TEM), electron energy loss spectroscopy (EELS), Auger electron spectroscopy (AES), current–voltage, and open circuit potential (OCP) measurements. The epitaxial GaN-InGaN interface, pseudomorphic InGaN thin films, homogeneous and suitable indium concentration and defined surface orientation are properties demanded for systematic study and efficient photoanodes based on III-nitride heterojunctions.

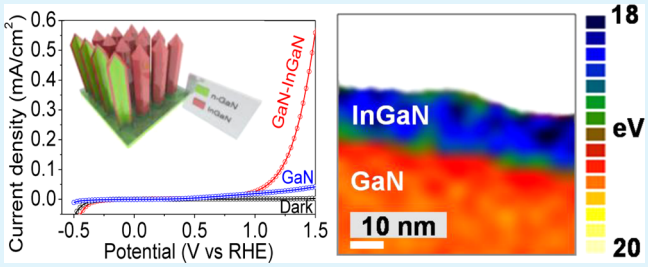

KEYWORDS: *GaN-InGaN heterostructure, transmission electron microscopy, electron energy loss spectroscopy, Auger electron spectroscopy, photoelectrochemical property, water splitting*

INTRODUCTION

Direct conversion of solar energy into hydrogen fuel by photoinduced water splitting is considered to be one of the most promising techniques to realize global renewable energy supply. To increase the efficiency of the photoelectrodes for water splitting, researchers are focusing on the development of suitable semiconductor materials, because the relevant energy levels have to be tuned by band gap engineering.[1−6] GaN-based material has been identified to be one of the promising candidates[7−9] because it has a relatively good chemical stability and its valence and conduction bands can be aligned with the water redox potentials, which is a prerequisite for efficient charge transfer between semiconductor and water-based electrolyte.[10] In addition, the GaN-InGaN system allows us to tune the band gap to adjust its spectral absorption to match the solar spectrum as well as to align the semiconductor bands close to the water redox potentials to achieve high efficiency.[11,12] Up to now, however, only a few studies employing GaN or InGaN for water splitting have been reported.[13−18] Thin films[13−16] suffer from high defect densities which might drastically reduce the photocurrent and hence the efficiency. In contrast to that, nanowires with high aspect ratio[17,18] have a much lower defect density and offer a higher active area. However, these nanowires are generally fabricated by a self-organized growth process, which might lead to low quality interfaces, inhomogeneous indium incorporation and uncontrolled crystal orientation, which are important parameters to influence the surface reactivity for hydrogen generation.[19] Therefore, it is difficult to draw distinct conclusions from the experiments reported so far. A strategy

Received: December 20, 2013
Accepted: February 11, 2014
Published: February 11, 2014

   dx.doi.org/10.1021/am4058937 | ACS Appl. Mater. Interfaces 2014, 6, 2235−2240

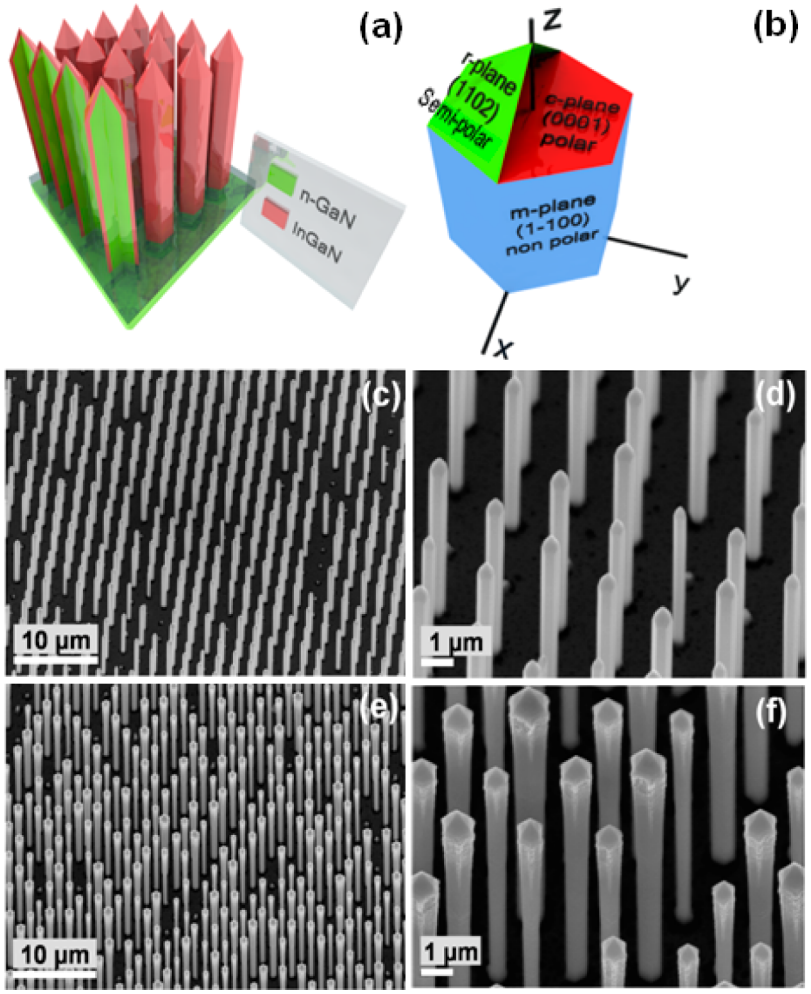

Figure 1. (a) Schematic illustration of MOVPE grown 3D GaN-InGaN core−shell rod arrays, used as photoanode for water splitting. (b) Polar and nonpolar facets of GaN rod crystal. (c) SEM image (30° tilted) of 3D GaN rods grown on a prepatterned template. (d) High-magnification SEM image (30° tilted) showing 3D GaN rods with hexagonal shapes. (e) SEM image (30° tilted) of 3D GaN rods coated with an ∼20 nm $In_{0.3}Ga_{0.7}N$ shell. (f) High-magnification SEM image (30° tilted) showing the 3D GaN-InGaN core−shell rods.

to develop new 3D GaN-InGaN-based photoanodes with controlled material properties is in great demand. Recently, the selected area growth (SAG) GaN 3D ensemble has become possible by major advancements in MOVPE growth technology.[20−22] Although the ordered 3D GaN rods have been intensively studied for growth mechanism and visible and ultraviolet light emitters during the last year,[22] few works have been reported about their potential for water splitting.

For the first time, we report water splitting results employing well aligned 3D GaN-InGaN rod arrays as photoanode with well-defined facet orientation. Other peculiarities of such photoanode are the epitaxial GaN-InGaN interface and the rather homogeneous indium content in the InGaN shell. The core−shell arrays, with aspect ratios up to 16 and indium content ca. 0.3, have been fabricated by MOVPE. A detailed structural analysis by HR-TEM, EELS, AES, current−voltage, and OCP measurements of the GaN-InGaN rod arrays are performed to characterize the structural and photoelectrochemical properties of our 3D GaN-InGaN photoanode.

RESULTS AND DISCUSSION

High-quality GaN-InGaN core−shell rod arrays were successfully grown on 2 in. prepatterned SiO_X-GaN/sapphire wafers by MOVPE. Figure 1a shows the schematic illustration of 3D GaN-InGaN core−shell rod arrays used as a photoanode for water splitting. The polar facets and the nonpolar m-plane {1−100} sidewalls of GaN crystal structure are shown in Figure 1b. N-type GaN rod arrays were grown on a prepatterned SiO_X-GaN/sapphire wafer and subsequently were coated by n-type InGaN layer (∼20 nm thick at half height of the rod) to fabricate GaN-InGaN arrays (experimental section, see the Supporting Information). To grow the epitaxial InGaN layer with high indium concentration on 3D GaN rods, low growth temperature and high indium precursor flow are required.

We studied the morphology, microstructure, and indium content of as-prepared GaN-InGaN samples by using scanning and transmission electron microscopy, electron energy loss, and Auger electron spectroscopy. Figure 1c−f show the morphologies of patterned GaN and GaN-InGaN arrays. The GaN arrays had an average diameter of 900 nm and 14 μm height. The aspect ratio of GaN rods was as high as 16. No growth took place on the SiO_2 mask, demonstrating excellent selectivity, whereas growth of GaN rods only took place in the mask openings. Figure 2a shows the cross-sectional TEM image of a single-crystalline GaN rod covered by an InGaN shell. Figure 2b displays a HR-TEM image of the GaN-InGaN interface. A selected area electron diffraction (SAED) pattern

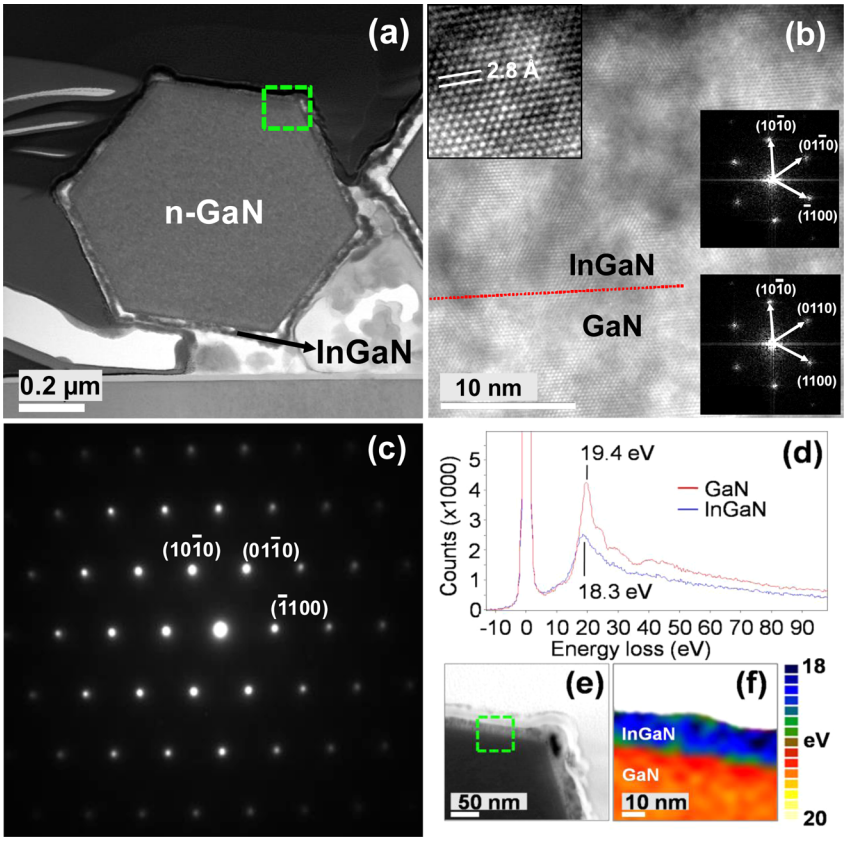

Figure 2. (a) Cross-sectional TEM image of the GaN-InGaN core−shell rod prepared by focused ion beam (FIB). (b) High-resolution TEM image of the GaN-InGaN interface (dotted range of a). InGaN lattice is shown in the inset. (c) SAED pattern corresponding to the core−shell rod in cross-section view. (d) EELS spectra of GaN and InGaN marked in red and blue color, respectively. (e) Cross-sectional TEM image of a GaN-InGaN rod and (f) plasmon energy map in the highlighted region showing the indium incorporation in the InGaN shell (see also Figure S2 in the Supporting Information).

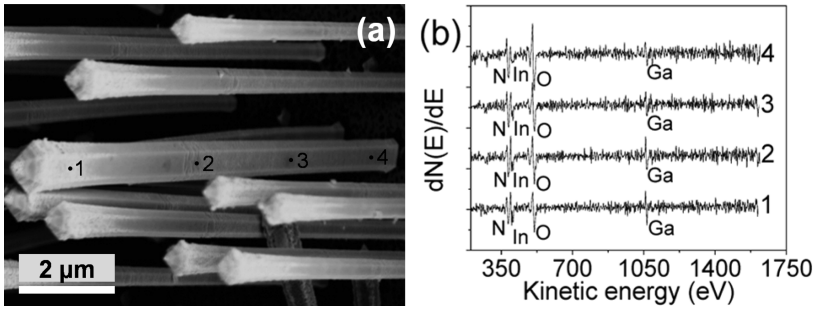

Figure 3. High-resolution Auger electron spectroscopy on a GaN-InGaN rod: (a) SEM image showing the probing positions and (b) the corresponding Auger spectra.

(Figure 2c) and Fourier analysis (FFT) of the HR-TEM images (inset, Figure 2b) reveal no splitting of the diffraction spots, thus confirming the epitaxial and the homogeneous growth of the InGaN on the GaN. The InGaN shell is pseudomorphically grown on the GaN core. HR-TEM and SAED observations yielded no evidence of interface dislocations (see Figure S1 in the Supporting Information). Figure 2d shows the EELS spectra of the GaN core and InGaN shell. The plasmon peaks at 18.3 and 19.4 eV can be assigned to $In_{0.3}Ga_{0.7}N$ and GaN, respectively. The main indium composition (0.30 ± 0.04) can be estimated by calculating the energy position of the plasmon peaks (see EELS in the Supporting Information).[23,24] The band gap (~2.36 eV) of $In_{0.3}Ga_{0.7}N$ leads to a compromise between the visible absorption of the solar spectrum and alignment of the energy levels with the water redox potentials.[10] TEM and EELS mapping images e and f in Figure 2 show the interface area between the GaN core and the InGaN shell. The InGaN mapping (blue) and a clear GaN-InGaN interface (orange-blue) reveal a radial indium variation less than 13% from the average value. Despite this small variation, the indium content of the $In_{0.3}Ga_{0.7}N$ shell can be retained rather homogeneous.

No phase segregation or dislocations at the interface were observed (Figure 2 and Figure S1 in the Supporting Information). Both the sidewalls of the GaN rods as well as $In_{0.3}Ga_{0.7}N$ shell layer exhibit nonpolar m-plane $\{1\bar{1}00\}$ orientation, so the chemical reactivity was dominated by the property of the nonpolar m-planes of InGaN. The EELS result shows that the indium concentration at the InGaN surface is

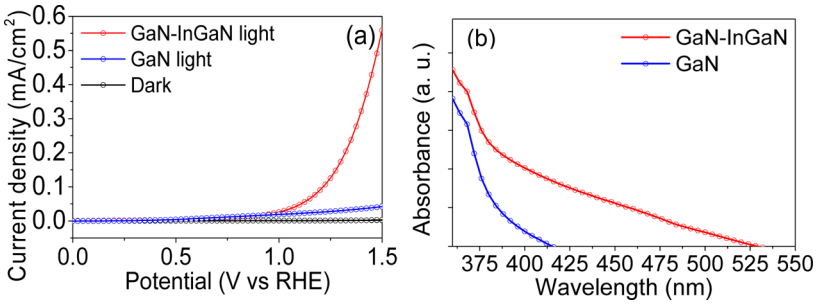

Figure 4. (a) Current density of 3D GaN-InGaN core–shell rod array (red) and 3D GaN rod array (blue) in 0.01 M H_2SO_4 solution under 100 mW/cm^2 illumination using AM 1.5 filter. (b) Optical absorbance curves of 3D GaN (blue) and 3D GaN-InGaN (red) rod arrays.

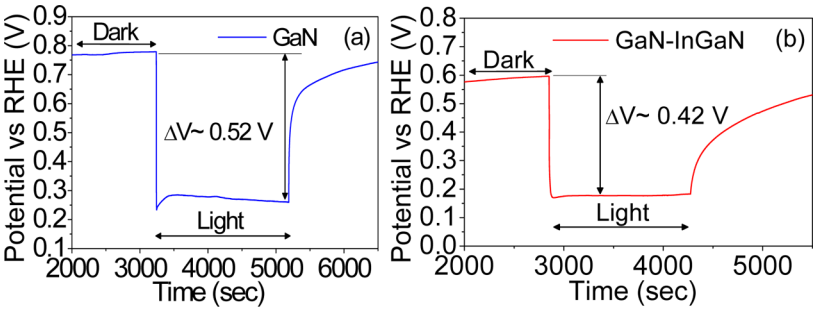

Figure 5. Open circuit potential (OCP) measurements on (a) GaN and (b) GaN-InGaN. The difference of potential between light and dark condition is negative, indicating n-type behavior.

similar to that in the InGaN bulk. At large scale (micrometers), AES nanoprobing allowed us to characterize the indium concentration at the surface along the rod axis. Panels a and b in Figure 3 show four AES probing positions along a single GaN-$In_{0.3}Ga_{0.7}N$ rod and the corresponding Auger electron spectra. A similar indium composition compared to EELS was derived from the AES data (see Table S1 in the Supporting Information).

The photoelectrochemical properties of GaN and GaN-$In_{0.3}Ga_{0.7}N$ rods were studied by current–voltage and open circuit potential (OCP) measurements. Figure 4a shows the photoelectrochemical measurement of GaN and GaN-$In_{0.3}Ga_{0.7}N$ rods under simulated solar light (AM1.5, 1 sun). The photocurrent density of GaN-$In_{0.3}Ga_{0.7}N$ increased to 0.3 mA/cm^2 (at 1.35 V) and was 10-fold higher than that of GaN rods (0.03 mA/cm^2 at 1.35 V). In both samples, the increase of the external potential led to an increase of the photocurrent density. The enhancement of the photocurrent GaN-$In_{0.3}Ga_{0.7}N$ is attributed to the extended light absorption of the $In_{0.3}Ga_{0.7}N$ shell in comparison to solely UV absorption of GaN rods. Because of the narrow band gap of the InGaN shells, a higher fraction of the visible and UV solar light is absorbed (Figure 4b) and an increased number of electron–hole pairs is generated (IPCE in Figure S3 in the Supporting Information). When the GaN-InGaN core–shell rods are in contact with the electrolyte, due to the semiconductor surface band bending, a driving force for the carrier separation is formed. The holes migrate toward the InGaN surface while the electrons route toward the GaN core. The GaN rod works as an electron collector because it is electrically conductive (see Figure S5 in the Supporting Information) and it transfers the electrons efficiently to the platinum counter electrode where protons are reduced to form gaseous H_2 (schematic in Figure S4 in the Supporting Information). The surface band bending was found to be dependent on Si concentration for GaN nanowires[25,26] and the high density of surface states on the m-plane.[27,28] Panels a and b in Figure 5 show the photovoltage measurements performed on GaN rods and GaN-InGaN rods, respectively. The open circuit potential (OCP) for GaN is 0.28 V and for GaN-InGaN is 0.18 V. Despite the large difference of conduction band edges of GaN and InGaN[10] the onset potentials of both systems are essentially similar. This feature could be attributed to the high density of surface states that could reduce the photovoltage or either pin the Fermi level for both GaN and GaN-InGaN electrodes.[29]

The photocurrent of our 3D GaN-InGaN was improved in comparison to Pendyala's and Hwang's reference works.[17,18] (i) A defined nonpolar surface; (ii) the epitaxial GaN-InGaN interface including nonrelaxed InGaN layers and (iii) a rather homogeneous and suitable indium concentration are certainly beneficial and necessary material properties to achieve high performance that must be taken into account.

One of the main limiting factors in semiconductor heterostructures for water splitting is the creation of multiple defects at their interfaces caused by the lattice-mismatch and nonepitaxial growth. These defects act as recombination centers that reduce the carrier lifetimes and the PEC photocurrent. In the case of our GaN-InGaN, there is no evidence of interfacial dislocations as demonstrated by HR-TEM (Figure 2b) and SAED (Figure 2c). Our GaN-InGaN ensemble shows an improved photocurrent density above 0.3 mA/cm^2 (at 1.35 V vs RHE), whereas in Hwang's work, this value was more than six times lower (0.05 mA/cm^2 at 1.35 V vs RHE). Although Si/InGaN hierarchical arrays[18] have larger surface than our GaN-InGaN arrays, the possible defects within the Si/InGaN interface due to the lattice mismatch (no info about the microstructures) could lower the photoanode performance. The homogeneous indium incorporation in GaN for suitable band engineering is another challenging issue, especially for 3D structures. In our case, a rather homogeneous indium

concentration in the $In_xGa_{(1-x)}N$ shells ($x \approx 0.30 \pm 0.04$) along the radial and longitude directions was achieved by MOVPE and confirmed by EELS mapping (Figure 2f) and Auger nanoprobing (Figure 3 and Table S1 in the Supporting Information), respectively. Furthermore, our 3D GaN-InGaN rod arrays is dominated by nonpolar m-plane $\{1\bar{1}00\}$ surfaces and minimized semipolar r-plane $\{1102\}$ (Figure 1b). The influence of polar InGaN surfaces on the water splitting can be excluded in our 3D GaN-InGaN system.[30]

The selected area growth (SAG) GaN-InGaN 3D rod arrays as an advanced photoanode have the following advantages: (i) defined morphology as test-bed for quantified PEC study depending on different geometrical parameters such as diameter, length and pitch; (ii) single-crystalline GaN-InGaN rod arrays with similar diameter and height; (iii) epitaxial GaN-InGaN interface, and (iv) suitable and rather homogeneous indium concentration in InGaN shell.

For InGaN, it is important to control the carrier concentration, the longitudinal shell thickness, as well as the density of surface states to achieve an efficient water splitting because these parameters affect the recombination process, the light absorption, as well as the space charge region.[25,26] Therefore, future studies will focus on the precise control and examination of carrier concentration of the GaN-InGaN during the growth process, the shell thickness variation, and the influence of surface states and their consequences on the water splitting performance. Another interesting study will be the enhancement of the light absorption over a broad wavelength range by optimizing the 3D geometry. MOVPE is a well-suited growth technique to address all these questions.

CONCLUSIONS

In summary, the 3D epitaxial GaN-$In_xGa_{1-x}N$ core−shell rod arrays with indium concentration of $x \approx 0.3$ has been successfully fabricated by MOVPE for visible light driven water splitting. Homogeneous indium incorporation in the InGaN shell was confirmed by EELS and Auger analysis. The 3D GaN-InGaN heterostructures show improved PEC properties compared to previously reported InGaN systems.[17,18] Certainly the high-quality epitaxial GaN-InGaN interface and dislocation free interface contributed to achieve an improved PEC property. Besides the controlled rod array pattern, the large active surface area, dislocation-free, and suitable indium concentration are particular advantages of 3D GaN-InGaN heterojunction systems for improved visible-light water splitting.

ASSOCIATED CONTENT

Supporting Information

The experimental section is added as well as TEM-EELS mapping description. Auger electron spectroscopy measurements, incident photon-to-current conversion efficiency spectra, and rod resistance measurement are also included. This material is available free of charge via the Internet at http://pubs.acs.org.

AUTHOR INFORMATION

Corresponding Authors

*E-mail: h.shen@tu-bs.de.
*E-mail: a.waag@tu-bs.de.

Author Contributions

The manuscript was written through contributions of all authors. All authors have given approval to the final version of the manuscript.

Notes

The authors declare no competing financial interest.

ACKNOWLEDGMENTS

The authors thank K.-H. Lachmund, D. Rümmler, A. Schmidt, J. Arens, M. Karsten, and W. Weiß for their technical support. H.S. is thankful to the BMBF-Nanofutur. The TEM and FIB facilities at CCiTUB are also acknowledged. J.M.R. acknowledges funding by the Spanish Government via a JAE-predoc grant. The authors thank Dr. A. Varea-Espelt and Dr. E. Xuriguera (MIND) for their scientific and technical support. The financial support of NTH is also gratefully acknowledged.

REFERENCES

(1) Hisatomi, T.; Dotan, H.; Stefik, M.; Sivula, K.; Rothschild, A.; Grätzel, M.; Mathews, N. Enhancement in the Performance of Ultrathin Hematite Photoanode for Water Splitting by an Oxide Underlayer. *Adv. Mater.* **2012**, *24*, 2699−2702.

(2) Paracchino, A.; Mathews, N.; Hisatomi, T.; Stefik, M.; Tilley, S. D.; Grätzel, M. Ultrathin Films on Copper (I) Oxide Water Splitting Photocathodes: a Study on Performance and Stability. *Energy Environ. Sci.* **2012**, *5*, 8673−8681.

(3) Dionigi, F.; Vesborg, P. C. K.; Pedersen, T.; Hansen, O.; Dahl, S.; Xiong, A.; Maeda, K.; Domen, K.; Chorkendorff, I. Gas Phase Photocatalytic Water Splitting with $Rh_{2-y}Cr_yO_3$/GaN:ZnO in μ-Reactors. *Energy Environ. Sci.* **2011**, *4*, 2937−2942.

(4) Li, J.; Hoffmann, M. W. G.; Shen, H.; Fàbrega, C.; Prades, J. D.; Andreu, T.; Hernandez-Ramirez, F.; Mathur, S. Enhanced Photoelectrochemical Activity of an Excitonic Staircase in CdS@TiO_2 and CdS@Anatase@Rutile TiO_2 Heterostructures. *J. Mater. Chem.* **2012**, *22*, 20472−20476.

(5) Fàbrega, C.; Andreu, T.; Tarancón, A.; Flox, C.; Morata, A.; Calvo-Barrio, L.; Morante, J. R. Optimization of Surface Charge Transfer Processes on Rutile TiO_2 Nanorods Photoanodes for Water Splitting. *Int. J. Hydrogen Energy* **2013**, *38*, 2979−2985.

(6) Fàbrega, C.; Andreu, T.; Güell, F.; Prades, J. D.; Estradé, S.; Rebled, J. M.; Peiró, F.; Morante, J. R. Effectiveness of Nitrogen Incorporation to Enhance the Photoelectrochemical Activity of Nanostructured TiO_2:NH_3 versus H_2−N_2 Annealing. *Nanotechnology* **2011**, *22*, 235403.

(7) Fujii, K.; Ohkawa, K. Bias-Assisted H_2 Gas Generation in HCl and KOH Solutions using n-Type GaN Photoelectrode. *J. Electrochem. Soc.* **2006**, *153*, 468−471.

(8) Kida, T.; Minami, Y.; Guan, G.; Nagano, M.; Akiyama, M.; Yoshida, A. Photocatalytic Activity of Gallium Nitride for Producing Hydrogen from Water under Light Irradiation. *J. Mater. Sci.* **2006**, *41*, 3527−3534.

(9) Waki, I.; Cohen, D.; Lal, R.; Mishra, U.; Denbaars, S. P.; Nakamura, S. Direct Water Photoelectrolysis with Patterned n-GaN. *Appl. Phys. Lett.* **2007**, *91*, 093519.

(10) Moses, P. G.; Miao, M.; Yan, Q.; Van de Walle, C. G. Hybrid Functional Investigations of Band Gaps and Band Alignments for AlN, GaN, InN, and InGaN. *J. Chem. Phys.* **2011**, *134*, 084703.

(11) Jampana, B. R.; Weiland, C. R.; Opila, R. L.; Ferguson, I. T.; Honsberg, C. B. Optical Absorption Dependence on Composition and Thickness of $In_xGa_{1-x}N$ ($0.05 < x < 0.22$) Grown on GaN/Sapphire. *Thin Solid Films* **2012**, *520*, 6807−6812.

(12) Murphy, A. B.; Barnes, P. R. F.; Randeniya, L. K.; Plumb, I. C.; Grey, I. E.; Horne, M. D.; Glasscock, J. Efficiency of Solar Water Splitting Using Semiconductor Electrodes. *Int. J. Hydrogen Energy* **2006**, *31*, 1999−2017.

(13) Li, J.; Lin, J. Y.; Jiang, H. X. Direct Hydrogen Gas Generation by using InGaN Epilayers as Working Electrodes. *Appl. Phys. Lett.* **2008**, *93*, 162107.
(14) Aryal, K.; Pantha, B. N.; Li, J.; Lin, J. Y.; Jiang, H. X. Hydrogen Generation by Solar Water Splitting using p-InGaN Photoelectrochemical Cells. *Appl. Phys. Lett.* **2010**, *96*, 052110.
(15) Mauder, C.; Tuna, Ö.; Gutrath, B.; Balmes, V.; Behmenburg, H.; Rzheutskii, M. V.; Lutsenko, E. V.; Yablonskii, G. P.; Noyong, M.; Simon, U.; Heuken, M.; Kalisch, H.; Vescan, A. Highly n-Type Doped InGaN Films for Efficient Direct Solar Hydrogen Generation. *Phys. Status Solidi* **2012**, *9*, 964−967.
(16) Theuwis, A.; Strubbe, K.; Depestel, L. M.; Gomes, W. P. A Photoelectrochemical Study of $In_xGa_{1-x}N$ Films. *J. Electrochem. Soc.* **2002**, *149*, 173−178.
(17) Pendyala, C.; Jasinski, J. B.; Kim, J. H.; Vendra, V. K.; Lisenkov, S.; Menon, M.; Sunkara, M. K. Nanowires as Semi-Rigid Substrates for Growth of Thick, $In_xGa_{1-x}N$ ($x > 0.4$) Epi-Layers without Phase Segregation for Photoelectrochemical Water Splitting. *Nanoscale* **2012**, *4*, 6269−6275.
(18) Hwang, Y. J.; Wu, C. H.; Hahn, C.; Jeong, H. E.; Yang, P. D. Si/InGaN Core/Shell Hierarchical Nanowire Arrays and their Photoelectrochemical Properties. *Nano Lett.* **2012**, *12*, 1678−1682.
(19) Fujii, K.; Iwaki, Y.; Masui, H.; Baker, T. J.; Iza, M.; Sato, H.; Kaeding, J.; Yao, T.; Speck, J. S.; Denbaars, S. P.; Nakamura, S.; Ohkawa, K. Photoelectrochemical Properties of Nonpolar and Semipolar GaN. *Jpn. J. Appl. Phys.* **2007**, *46*, 6573−6578.
(20) Wang, X.; Li, S.; Fündling, S.; Wei, J.; Erenburg, M.; Wehmann, H.-H.; Waag, A.; Bergbauer, W.; Strassburg, M.; Jahn, U.; Riechert, H. Polarity Control in 3D GaN Structures Grown by Selective Area MOVPE. *Cryst. Growth Des.* **2012**, *12*, 2552−2556.
(21) Wang, X.; Li, S.; Mohajerani, M. S.; Ledig, J.; Wehmann, H.-H.; Mandl, M.; Strassburg, M.; Steegmüller, U.; Jahn, U.; Lähnemann, J.; Riechert, H.; Griffiths, I.; Cherns, D.; Waag, A. Continuous-Flow MOVPE of Ga-Polar GaN Column Arrays and Core − Shell LED Structures. *Cryst. Growth Des.* **2013**, *13*, 3475−3480.
(22) Li, S.; Waag, A. GaN Based Nanorods for Solid State Lighting. *J. Appl. Phys.* **2012**, *111*, 071101.
(23) Egerton, R. F. *Electron Energy-Loss Spectroscopy in the Electron Microscope*; Plenum Press: New York, 1996.
(24) Eljarrat, A.; Estradé, S.; Gačević, Ž.; Fernández-Garrido, S.; Calleja, E.; Magén, C.; Peiró, F. Optoelectronic Properties of InAlN/GaN Distributed Bragg Reflector Heterostructure Examined by Valence Electron Energy Loss Spectroscopy. *Microsc. Microanal.* **2012**, *18*, 1143−1154.
(25) AlOtaibi, B.; Harati, M.; Fan, S.; Zhao, S.; Nguyen, H. P. T.; Kibria, M. G.; Mi, Z. High Efficiency Photoelectrochemical Water Splitting and Hydrogen Generation using GaN Nanowire Photoelectrode. *Nanotechnology* **2013**, *24*, 175401.
(26) Wallys, J.; Hoffmann, S.; Furtmayr, F.; Teubert, J.; Eickhoff, M. Electrochemical Properties of GaN Nanowire Electrodes - Influence of Doping and Control by External Bias. *Nanotechnology* **2012**, *23*, 165701.
(27) Ivanova, L.; Borisova, S.; Eisele, H.; Dähne, M.; Laubsch, A. Ebert, Ph. Surface States and Origin of the Fermi Level Pinning on Nonpolar GaN (1−100) Surfaces. *Appl. Phys. Lett.* **2008**, *93*, 192110.
(28) Van de Walle, C. G.; Segev, D. Microscopic Origins of Surface States on Nitride Surfaces. *J. Appl. Phys.* **2007**, *101*, 081704.
(29) Veal, T. D.; Jefferson, P. H.; Piper, L. F. J.; McConville, C. F.; Joyce, T. B.; Chalker, P. R.; Considine, L.; Lu, H.; Schaff, W. J. Transition from Electron Accumulation to Depletion at InGaN Surfaces. *Appl. Phys. Lett.* **2006**, *89*, 202110.
(30) Chen, P.-T.; Sun, C.-L.; Hayashi, M. First-Principles Calculations of Hydrogen Generation Due to Water Splitting on Polar GaN Surfaces. *J. Phys. Chem. C* **2010**, *114*, 18228−18232.